Biopalaeogeography

Mesoproterozoic biomineralization: Cyanobacterium-like filamentous siderite sheaths ~1.4 Ga

Dong-Jie Tang [a,b,], Xiao-Ying Shi [a,c], Xi-Qiang Zhou [d,e], Robert Riding [f]*

[a] *State Key Laboratory of Biogeology and Environmental Geology, China University of Geosciences (Beijing), Beijing 100083, China*
[b] *Institute of Earth Sciences, China University of Geosciences (Beijing), Beijing 100083, China*
[c] *School of Earth Sciences and Resources, China University of Geosciences (Beijing), Beijing 100083, China*
[d] *Key Laboratory of Cenozoic Geology and Environment, Institute of Geology and Geophysics, Chinese Academy of Sciences, Beijing 100029, China*
[e] *College of Earth and Planetary Sciences, University of Chinese Academy of Sciences, Beijing 100049, China*
[f] *Department of Earth and Planetary Sciences, University of Tennessee, Knoxville, TN 37996-1526, USA*

Abstract   Biomineralization was a key development in a wide variety of organisms, yet its history prior to the Ediacaran remains poorly understood. In this paper, we describe ~1420—1330 million year old microscopic tubes preserved as siderite ($FeCO_3$). In size and shape these tubes closely resemble cyanobacterial sheaths forming mineralized mats. We consider two competing explanations for their formation. First, the tubes and associated sediment were originally composed of Ca-carbonate that was subsequently replaced by siderite. In this case, siderite mineralization was early, but post-mortem, as in early silicification, and preferentially preserved the more resilient sheath. However, no relict calcite is observed. Second, the Fe-carbonate mineralogy of the tubes and sediment is synsedimentary. In this case, photosynthetic oxygen may have precipitated Fe-oxyhydroxide that was promptly converted to siderite by dissimilatory iron reduction (DIR). Primary siderite mineralization of cyanobacteria has not been described before. Both explanations link photosynthetic processes to preferential sheath mineralization during the life of the cyanobacteria, as observed in present-day calcified cyanobacteria. This process might include CO_2-concentrating mechanisms (CCMs) linked to relatively low levels of atmospheric CO_2, consistent with empirical estimates of mid-Proterozoic CO_2 levels based on paleosols and weathering rinds. In either case, these cyanobacterium-like fossils preserved in siderite provide an early example of biomineralization and suggest the interactive influences of both metabolic processes and ambient seawater chemistry.

Keywords   Xiamaling Formation, Siderite, Ferruginous, Dissimilatory iron reduction (DIR), Iron formation (IF), CO_2-concentrating mechanism (CCM)

1.   Introduction

Biomineralization, the ability to influence and direct mineral precipitation, occurs in virtually all major groups of organisms (Leadbeater and Riding, 1986; Lowenstam and Weiner, 1989) and was a key evolutionary innovation (e.g., Knoll, 2003; Wood, 2018). In addition to providing strength, protection, support, environmental sensing and chemical storage (Mann, 1988; Cuif *et al.*, 2010), it is commonly linked to major — often essential — adaptations that utilize a wide range of biomolecules in the regulation and mediation of complex processes (Mann, 2001). From the geological perspective, the widespread biological precipitation of $CaCO_3$ (Meldrum, 2003) has significantly contributed to global elemental cycling over geological timescales, influencing both Earth surface climate and sedimentation (Cohen and McConnaughey,

2003; Knoll, 2003; Weiner and Dove, 2003; Livingston *et al.*, 2006; Gal *et al.*, 2015; Drake *et al.*, 2020). Biomineralization is widely regarded as a signature feature of Phanerozoic history, directly responsible for a rich and detailed marine fossil record that has, in turn, contributed to the precipitation of significant volumes of $CaCO_3$ and silica by invertebrates and algae (Knoll, 2003).

Biomineralization provides support and protection for diverse organisms (Westbroek and De Jong, 1983; Leadbeater and Riding, 1986). The intensification of biomineralization during Late Proterozoic and Early Paleozoic invertebrate diversification (Knoll, 2003; Murdock, 2020) strongly suggests links with protection from predation (Wood, 2018). From a utilitarian perspective, it would be tempting to regard biomineralization as a purposeful enterprise centered on protection and support. However, this may not fully account for the origins of biomineralization, since it is
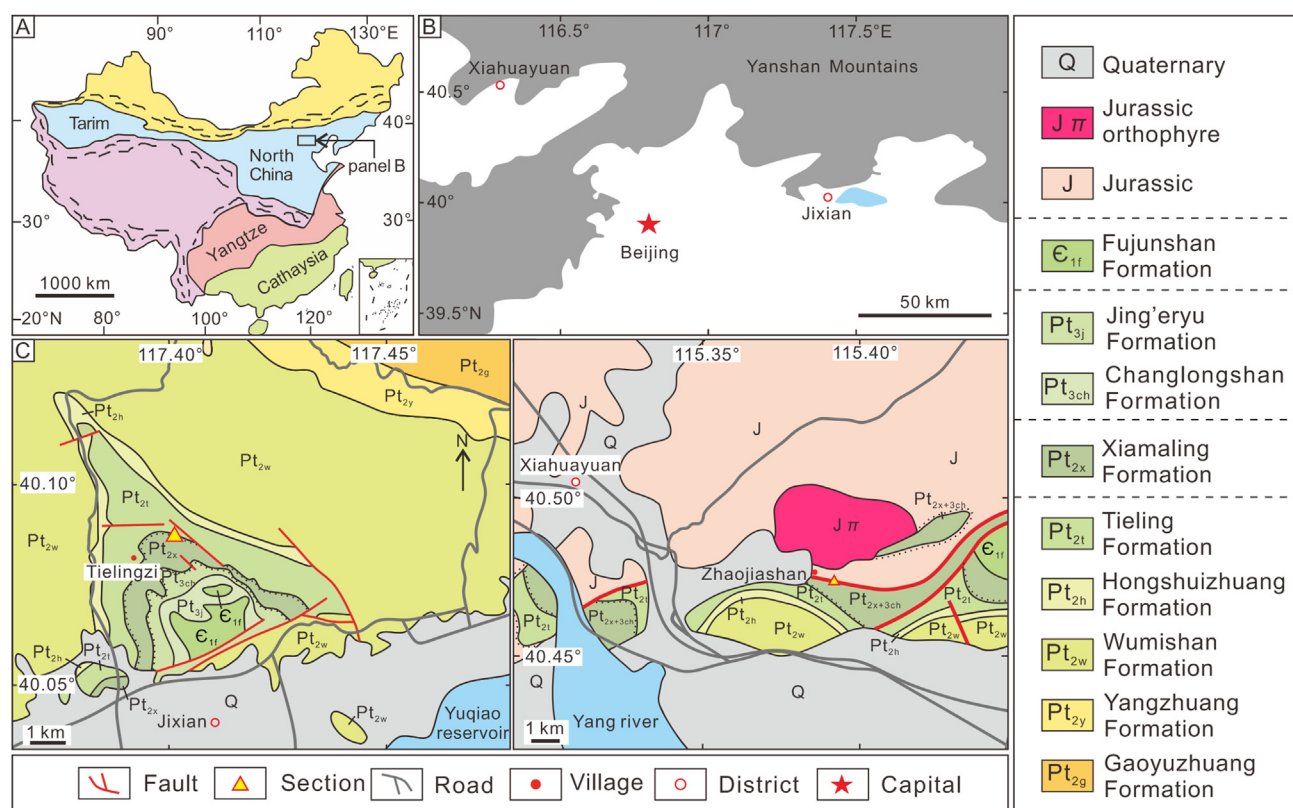
Fig. 1 Geological setting and sampling location. **A)** Major tectonic subdivisions of China and location of the study area; **B)** Simplified map showing the location of the study area; **C)** and **D)** Simplified geological maps of the studied sections (modified from HBGMR, 1965 and HBGMR, 1967, respectively). Dashed lines between formations indicate disconformities.

evident that its processes are deeply rooted in nano-materials (Krajina *et al.*, 2018) '*that naturally assemble themselves*' (Viney, 2004). For this reason, it is important to identify and understand early examples of biomineralization (Porter *et al.*, 2003; Cohen *et al.*, 2017) to address questions regarding its origins, role and significance.

Here we describe ~1.4 Ga tubular filaments from the Jixian area of northern China (Fig. 1) that are composed of siderite. In overall size and morphology they resemble the sheaths of cyanobacteria. Their siderite composition may have involved bacterial metabolisms, such as oxygenic photosynthesis, Fe-oxidation and DIR. These microscopic tubes are not the oldest fossils resembling mineralized bacteria (Klein *et al.*, 1987), but they are exceptionally well preserved and, so far as we are aware, are the first fossil siderite tubes of this type to be described.

2.   Geological setting

The Mesoproterozoic Xiamaling Formation is dominated by dark siltstones and shales (Zhang *et al.*, 2016; Tang *et al.*, 2017, 2018, 2020a; Liu *et al.*, 2019, 2020a) divisible into four members (I to IV) that constitute a large-scale transgressive-regressive cycle, with the deepest water deposition in Member III (Fig. 2; Tang *et al.*, 2017). The middle part of the Formation has been suggested to have mainly been deposited below storm-wave base (Meng *et al.*, 2011; Zhang *et al.*, 2016). In the studied Jixian section, the Xiamaling Formation disconformably overlies the Tieling Formation and only Member I is preserved (Figs. 2 and 3A). The upper member of the Tieling Formation is composed of stromatolitic limestone dominated by carbonate mud. This mud is generally well-preserved and is interpreted to mainly be a water-column precipitate (Tosti and Riding, 2017; Wu *et al.*, 2021). The Xiamaling Formation consists of three parts (Fig. 2; Ma *et al.*, 2022): (i) Lowermost: alternating reddish mudstone and green to grey muddy siltstone rich in glauconite, berthierine and chamosite (0—1.5 m); (ii) Lower: grey to black silty shale with abundant siderite concretions and siderite grainstone-bands (1.5 m—17 m; Fig. 3B and C); and, (iii) Middle to Upper: green silty shale with numerous cross-bedded quartz sandstone bands (17 m—160 m). Taken as a whole, these deposits are broadly interpreted to reflect an offshore transitional environment near and below fair-weather wave base (Ma *et al.*, 2022). The grainstone bands are commonly <3 m in width and <10 cm in thickness (Fig. 3B and C), and are likely storm deposits that were transported from shallower environments. There can be up to eight bands in a 1-m-interval, suggesting frequent storm influence. Abundant fossils occur in these siderite grainstone bands but no fossils have been identified in the siderite concretions. Paleogeographically, the Xiamaling Formation formed in an environmental setting that was likely linked to the open ocean throughout its depositional history (Zhang *et al.*, 2019).

The Xiamaling sediments in northern China are generally well preserved. Maturation studies of the organic matter indicate that the sediments underwent relatively low thermal evolution, with burial temperatures ≤90 °C (Zhang *et al.*, 2015; Luo *et al.*, 2015). Similarly, the polytypes of Xiamaling chamosites are essentially I*bb*, indicating a burial depth <2000 m, corresponding to a burial temperature of <80 °C (Tang *et al.*, 2017). Biomarkers extracted from Xiamaling black shale suggest that the organic matter was primarily derived from prokaryotes, with cyanobacteria as the major biomass, and also shows low thermal maturity in the early to middle oil window (Luo *et al.*, 2015).

The Xiamaling Formation disconformably overlies the Tieling Formation (Jixian Group) and is overlain by the Changlongshan Formation of the Qingbaikou Group (Fig. 2). Zircon and baddeleyite ages are 1418 ± 14 Ma for the lower part of Member 1 (Lyu *et al.*, 2021), 1392.2 ± 1.0 Ma and 1384.4 ± 1.4 Ma for the middle part of the Formation (Zhang *et al.*, 2015), and 1330—1305 Ma for diabase sills in the upper part of the Formation (Zhang *et al.*, 2017). These data suggest an overall age for the Xiamaling Formation within the range ~1.42—1.33 Ga. The fossils described here, from an interval near the base of the formation, therefore appear to have an approximate age of 1.4 Ga.

3.   Material and methods

Twenty-five samples were collected from Member I of the Xiamaling Formation along freshly exposed road cuts near Tielingzi village (40°05′16.68″N, 117°24′7.95″E), ~95 km east of Beijing (Figs. 1 and 2). Samples were cut into chips and only the fresh central parts were used for mineralogical/geochemical analyses and thin section preparation. Prior to analysis, the samples were cleaned, dried and ground to powder (~200 mesh) in an agate mortar to avoid contact with metals. Macroscopic features were observed in the field and microfabrics were examined microscopically in thin-sections. Ultra-structures were investigated in thin sections using a Zeiss Supra
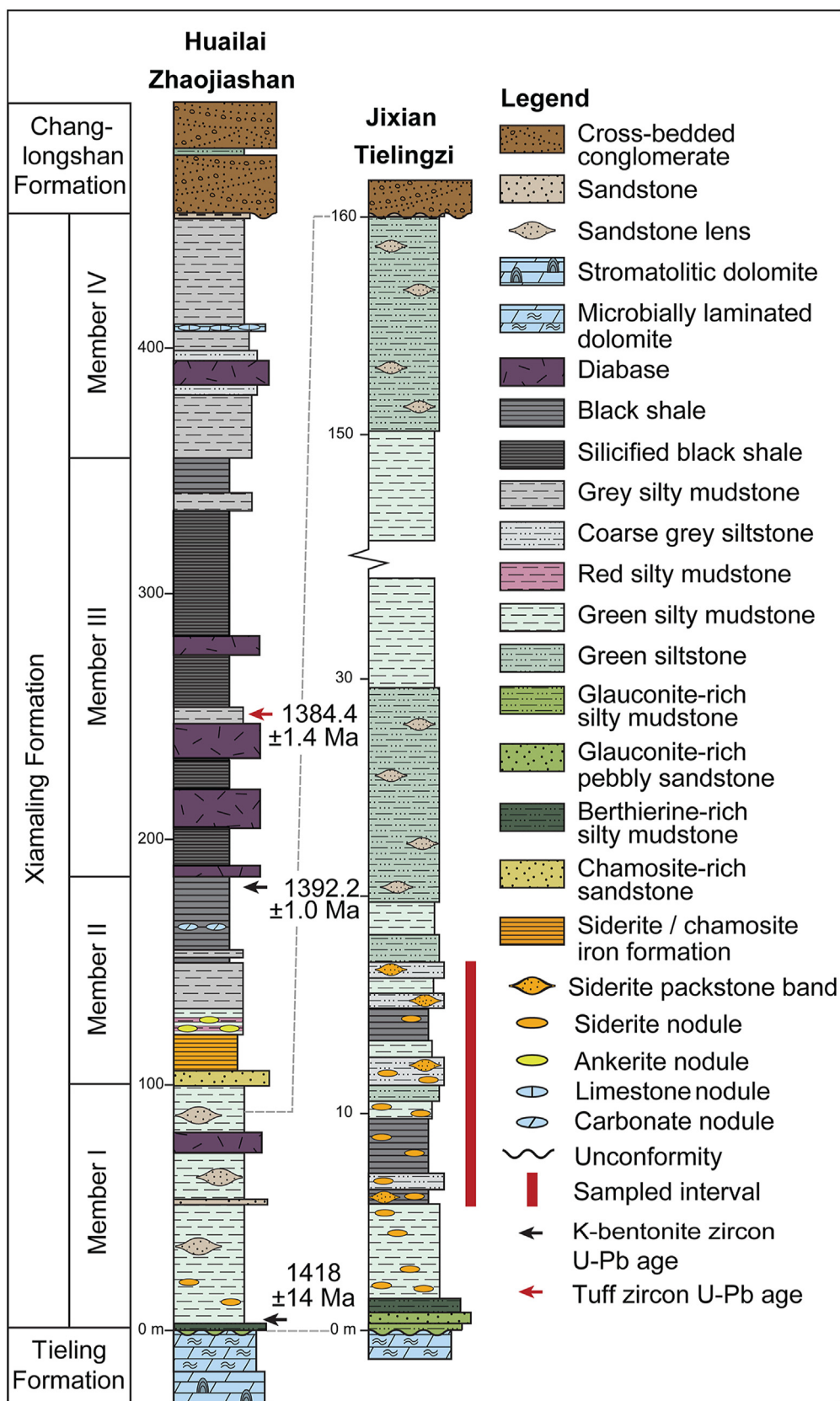
Fig. 2 Stratigraphic columns of the Xiamaling Formation at Zhaojiashan village, Huailai County and Tielingzi village, Jixian County, Northern China (modified from Ma *et al.*, 2022), showing the studied interval and the boundary between the siliciclastic-dominated Xiamaling Formation and the carbonate-dominated Tieling Formation. In the Jixian section, the upper part of Member I of the Xiamaling Formation is not preserved; correlation between the Jixian and Huailai sections is estimated. The geochronological constraints are adopted from Zhang *et al.* (2015) and Lyu *et al.* (2021).

Fig. 3 Major depositional characteristics of Member I of the Xiamaling Formation and the underlying Tieling Formation in the Jixian section near Tielingzi village, Jixian County, northern China. **A)** Disconformable boundary between the Tieling and Xiamaling formations. The upper Tieling Formation is dominated by stromatolitic limestone, while the basal Xiamaling Formation consists of iron-rich silty mudstone and siltstone; **B)** Grey silty shale interbedded with siderite-grainstone bands (arrowed) containing abundant *Xiamalingella* siderite tubes; **C)** Close view of a siderite-grainstone band (black-white arrow) that contains *Xiamalingella* tubes, and of siderite-nodules (red-yellow arrow) that lack *Xiamalingella*, in silty shale.

55 field emission scanning electron microscope (FESEM) under 20 kV accelerating voltage with a working distance of ~15 mm. A secondary electron imaging detector (SE2) was used to characterize topographic features, and an AsB detector was used to reveal compositional differences (backscattered electron, BSE, image). Samples were coated with ~8-nm-thick carbon prior to analysis. Elemental concentrations of micron-sized spots were semi-quantitatively analyzed using an energy dispersive X-ray spectrometer (EDS) connected to the FESEM, operated at 20 kV with a working distance of ~15 mm. For carbon isotope analyses, sample powders were drilled from polished slabs, avoiding weathered surfaces and recrystallized areas.

The C—O isotope analyses were conducted at the State Key Laboratory of Biogeology and Environmental Geology, China University of Geosciences (Wuhan). About 150 μg—400 μg of powder was placed in a 10 mL Na-glass vial, sealed with a butyl rubber septum, and reacted with 100% phosphoric acid at 72 °C after flushing with helium. The evolved CO_2 gas was analyzed for $\delta^{13}C$ and $\delta^{18}O$ using a MAT 253 mass-spectrometer coupled directly to a Finnigan Gas-bench II interface (Thermo Scientific). Isotopic values are reported as per mille relative to the Vienna Pee Dee belemnite (V-PDB) standard. Analytical precision was better than ±0.1‰ for $\delta^{13}C$ and ±0.1‰ for $\delta^{18}O$, based on replicate analyses of two laboratory standards (GBW 04416 and GBW 04417).

4. Results and discussion

4.1. Mineralization of cyanobacterial sheaths

Xiamalingella filaments (see **5 Systematic paleontology**) are closely interwoven in mat-like bundles and appear benthic (Fig. 4A—F). In detail, the tube walls are fine-grained siderite (Fig. 4E—H) with black grains resembling iron minerals (Fig. 4F). They have been preserved by impregnation with a fine-grained mineral which is now, and may originally have been, siderite. Small filaments have commonly been described from grains in cherts (e.g., Zhao *et al.*, 2020), as well as from phosphorites (e.g., She *et al.*,
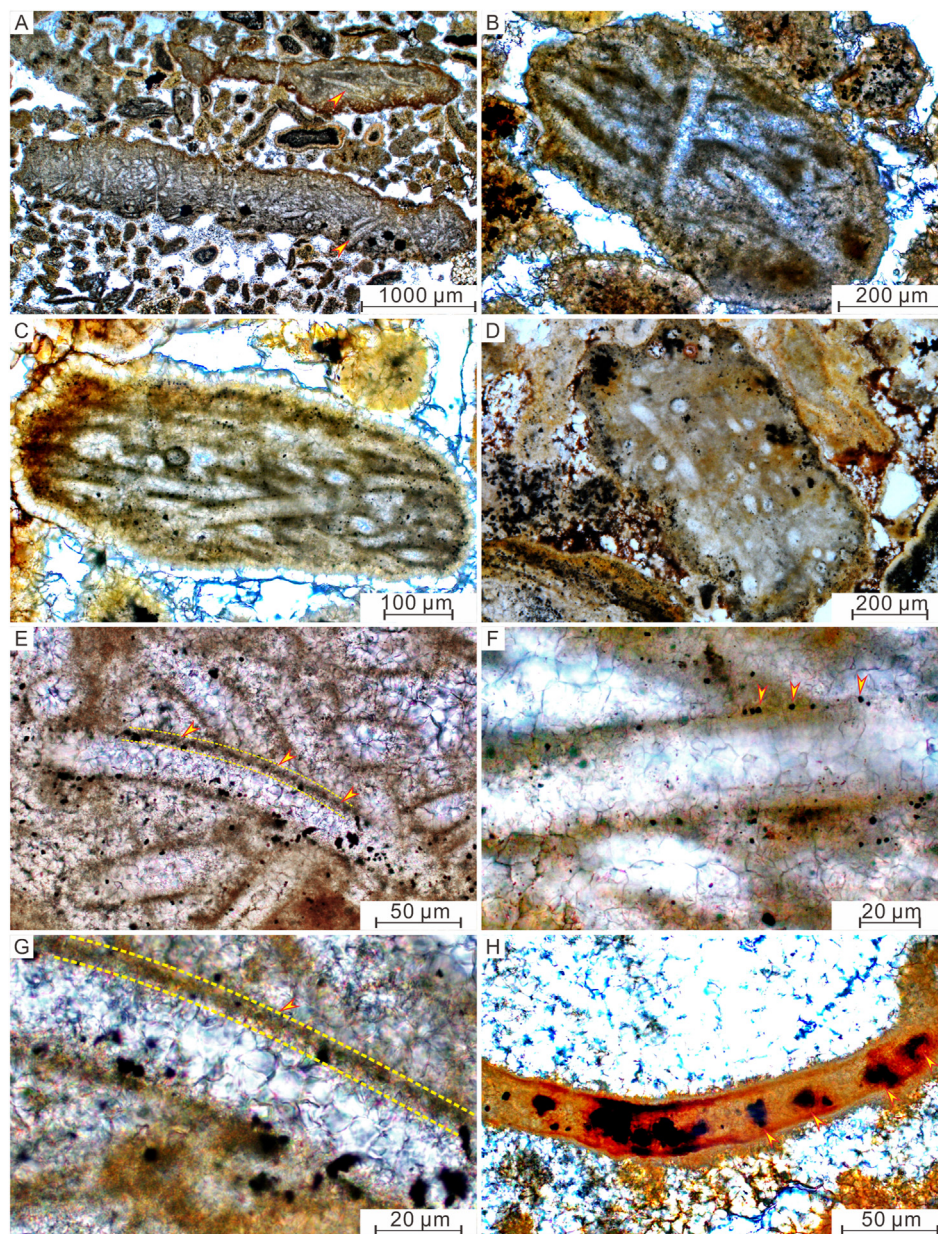
Fig. 4 Microscopic features of *Xiamalingella* filaments in siderite bioclastic grainstone from the Lower Xiamaling Formation. **A—C)** Abundant filaments in siderite grainstone clasts (arrows); **D)** Interwoven arrangement showing filaments with circular cross-sections and well defined walls; **E)** Microscopic features of siderite tubes, showing their sheaths with constant thickness (arrows and dashed lines); **F)** Siderite tubes with dark mineral inclusions in the walls (arrows); **G)** Enlargement of panel **E**, showing the small mineral size in the sheath (arrow and dashed lines) compared to the cement filling the tube; **H)** Siderite tube containing dark minerals (arrows), possibly resembling mineralized cell material.

2013, figure 2j) and iron formation (e.g., Dodd *et al.*, 2018, figure 9), and some of these granules are sideritic (e.g., Stefurak *et al.*, 2014, figure 1).

In our samples, tubes, associated matrix and diagenetic cement are all siderite, with low Ca concentrations (Fig. 5) and negative carbon isotope values of the bulk rock (<−10‰; Table 1). The morphological decomposition of cyanobacteria is commonly a rapid process, and could occur on a time scale of days to weeks (Bartley, 1996). In this study, the individual sheaths are well preserved with relatively constant thickness (Fig. 4), suggesting synsedimentary sheath mineralization. We consider two possible explanations for the primary composition of *Xiamalingella* tubes: calcite ($CaCO_3$) (Fig. 6A) and siderite ($FeCO_3$) (Fig. 6B and C; adapted from Riding, 2006).

Fig. 5 Composition of cyanobacterial filaments in siderite bioclastic grainstone from the Lower Xiamaling Formation. **A)** Siderite grain containing abundant filaments; **B)** BSE image, showing the compositional difference between the sheaths and the tube-fills; **C)** Enlargement of filaments in **B**, showing dark colored sheaths with constant thickness (arrowed); **D)** and **E)** EDS spectra, showing sheaths composed of Mn-rich micritic siderite, and tubes composed of Fe-rich siderite; **F–H)** EDS element mapping of **B**, showing Fe, Mn and Ca distribution; the sand grains are siderite with high Fe concentration and low Mn and Ca concentrations; the tubes are Fe-rich but Mn-poor, the sheaths are Fe-poor and Mn-rich.

Sample ID	$\delta^{13}C$ (PDB)‰	$\delta^{18}O$ (PDB)‰
1707XML-06	−12.8	−4.4
1707XML-07	−10.3	−9.4
1707XML-13	−11.3	−4.4
1807TLZ-09.5m	−10.5	−4.6
1807TLZ-11.8m	−10.9	−5.1

4.2. Primary CaCO₃

In vivo cyanobacterial sheath calcification can occur under conditions that favor the precipitation of $CaCO_3$ minerals, and does not appear to be obligatory (Riding, 2006). It is best known at the present day in freshwater streams (Merz-Preiß and Riding, 1999; Pentecost, 2005), and is relatively rarely reported from present-day marine environments (Riding, 1991; Planavsky et al., 2009). Nonetheless, calcified cyanobacterial sheath microfossils have a good geological record, albeit strongly fluctuating in abundance, which ranges from common (e.g., Early Paleozoic, Devonian/

Carboniferous, Late Jurassic/Early Cretaceous) to scarce (e.g., much of the Late Cretaceous and Cenozoic) (Arp et al., 2001). This distribution has been suggested to relate to fluctuations in the propensity of seawater to precipitate $CaCO_3$ and also to the ability of cyanobacteria to utilize CO_2-concentrating mechanisms (CCMs) at times of relatively low aqueous CO_2 concentrations (Thompson and Ferris, 1990; Merz, 1992; Kempe and Kazmierczak, 1994; Riding, 2006). Thus, when carbon dioxide levels are relatively low, as at the present-day, cyanobacteria can utilize HCO_3^- as an additional source of dissolved inorganic carbon (Riding, 1991; Planavsky et al., 2009). The intracellular processes that convert bicarbonate to carbon dioxide [HCO_3^- (absorbed from ambient water) → CO_2 (used by cyanobacteria) + OH^- (released to sheath)] result in localized increase in extracellular pH adjacent to the cells, which, if local environmental conditions are favorable, can lead to $CaCO_3$ precipitation on and in the sheath (Merz-Preiß and Riding, 1999; Riding, 2006). Sheath structure may also favor calcification (Golubic and Seong-Joo, 1999).
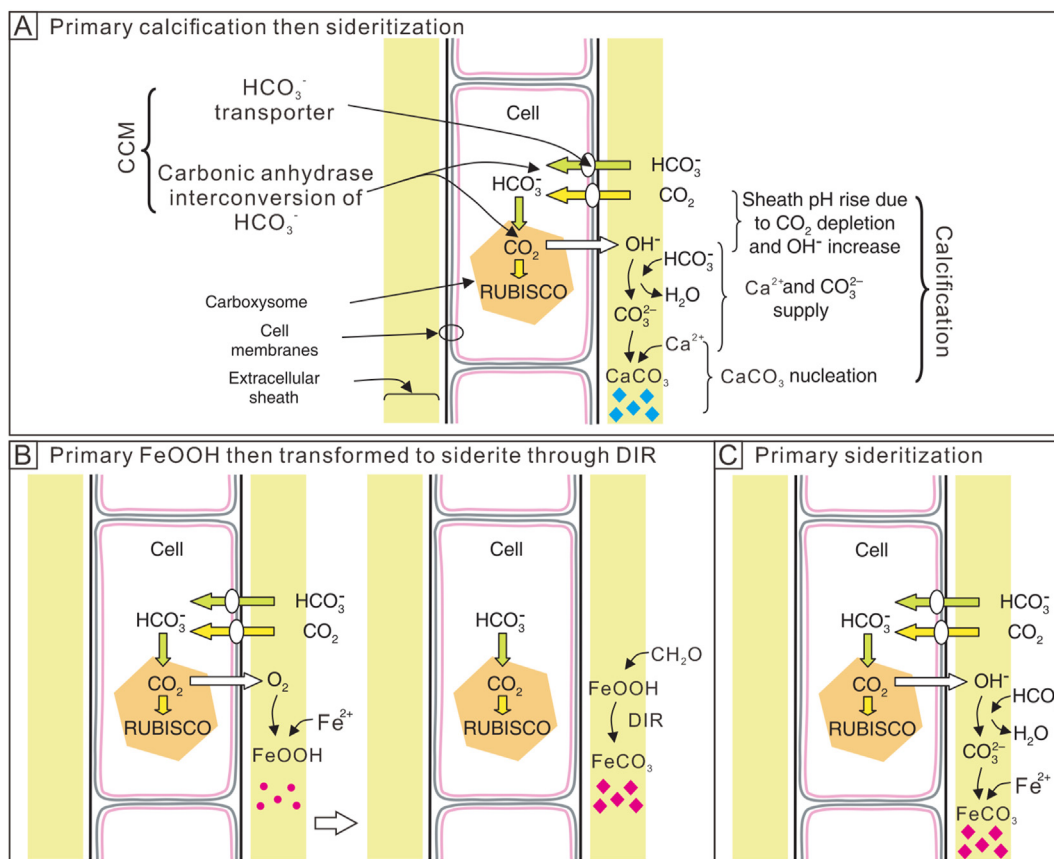
Fig. 6 Speculative biomineralization pathways for *Xiamalingella* (adapted from Riding, 2006, figure 3) **A)** *In vivo* cyanobacterial sheath calcification through the CO_2-concentrating mechanism (CCM). This could then be followed by transformation into siderite during diagenesis, by a process similar to silicification; **B)** Oxidation of Fe(II) in sheaths by oxygen produced by photosynthesis during illumination, subsequently transformed into siderite by dissimilatory iron reduction (DIR) during darkness; **C)** Direct sideritization of sheaths due to pH increase induced by CCM.

Proterozoic examples of calcified cyanobacterial sheaths are mainly *Girvanella*-like forms, e.g., ~1200 Ma Society Cliffs Formation (Kah and Riding, 2007; subdivided into Iqqittuq, Angmaat, Nanisivik, and Ikpiarjuk formations by Turner, 2009), ~890 Ma Little Dal (Turner et al., 1993; age from Turner, 2021), 750—700 Ma Draken Group (Swett and Knoll, 1985; Fairchild et al., 1991; Knoll et al., 1989, 1991, 1993). Coiled filaments, similar in form to present-day *Spirulina*, occur widely in the Neoproterozoic, variously preserved in pyrite, phosphate and silica, and are generally referred to *Obruchevella* (Knoll and Ohta 1988; Peel, 1988; Mankiewicz, 1992; Buick and Knoll 1999; Sergeev and Schopf, 2010; Moore et al., 2017). In addition, late Ediacaran phosphatic filamentous fossils associated with *Obruchevella* in Shaanxi, China, have been compared with *Girvanella* and *Subtifloria* and also include *Rivularia*-like *Cambricodium* (Min et al., 2020).

If siderite fully replaced the original minerals without leaving any relics, then it is possible that *Xiamalingella* tubes and associated sediment were originally $CaCO_3$ and were subsequently synsedimentary diagenetically converted to siderite. In this case, sheath calcification could have occurred by the mechanism that has been inferred for other Proterozoic examples (Riding, 2006; Kah and Riding, 2007), i.e., increase in ambient pH due to CCM, connected with oxygenic photosynthesis, promoted *in vivo* sheath calcification. These processes could have occurred under overall oxygenated conditions. Subsequent upward oxycline migration in seawater associated with ferruginous conditions could have promoted synsedimentary sideritization of these originally calcareous tubes and sediment.

Siderite can be formed through primary, early diagenetic or late diagenetic processes (Tang et al., 2018 and references therein). However, EDS analysis of *Xiamalingella* shows Ca content less than 1 wt% (Fig. 5D and E). BSE images and EDS analysis results indicate that the sheaths are composed of Mn-rich micritic siderite with constant thickness, while tubes are infilled by Fe-rich siderite with larger grain size (Fig. 5). In diagenetic siderite, Ca contents can be up to 4 wt% (Tang et al., 2018, Fig. 6A). The low values of Ca observed in the *Xiamalingella* tubes therefore suggest an original composition that was unlikely to have been $CaCO_3$.

4.3. Synsedimentary siderite

The *Xiamalingella* tubes, together with the surrounding matrix and cements, are all siderite (Fig. 5). The tube-wall (interpreted as the sheath) is Mn-rich rather than Ca-rich and no calcite relics have been observed (Fig. 5), suggesting that the siderite is synsedimentary. The formation of siderite requires anoxic and Fe-rich conditions with high alkalinity but low sulfate concentrations (e.g., Tang et al., 2018). The occurrence of abundant glauconite- and berthierine-rich siltstone also indicates anoxic and ferruginous conditions (Ma et al., 2022). Therefore, if siderite was the primary mineral, then O_2 must have been low or was consumed very quickly. If oxygen was produced by photosynthesis then, in this ferruginous environment, Fe-oxyhydroxide should have formed. However, we find no evidence of original Fe-oxyhydroxide in the sheath. If it was originally present, it could have been consumed by synsedimentary DIR and either removed in solution or precipitated as siderite, which is supported by the negative carbon isotope composition (Table 1; cf. Tang et al., 2018). This permits the possibility that the siderite could have been primary or early diagenetic and was bacterially produced by DIR. Primary precipitation of siderite has rarely been described, while the early diagenetic formation of stratiform siderite through DIR has been reported in Member II of the Xiamaling Formation (Tang et al., 2018). In this study, we envisage the following possible sequence of fabric development in the siderite grainstone containing *Xiamalingella* from Member I of the Xiamaling Formation (Fig. 6B and C).

i) Within diurnal light-dark cycles, amorphous Fe(III) oxyhydroxide precipitated during illumination in the cyanobacterial sheaths as a result of oxygenic photosynthesis (e.g., Swanner et al., 2017). If the cyanobacteria were utilizing a CCM then this could have produced OH^- in the sheath that promoted siderite as well as Fe(III) oxyhydroxide precipitation.

ii) DIR continuously converted Fe-oxyhydroxide to siderite (Rose and Waite, 2005; Lis and Shaked, 2009; Rudolf et al., 2015; Thorne et al., 2015), possibly as: $4Fe(OH)_3 + CH_2O + 3HCO_3^- \rightarrow 4FeCO_3 + 3OH^- + 7H_2O$ (Heimann et al., 2010; Tang et al., 2018). This process preserved the organic sheaths as siderite tubes, and resulted in the negative composition of the carbon isotopes.

iii) The mineralized sheaths and associated grains were synsedimentarily cemented by siderite.

iv) Currents eroded and transported the sediment, reworking the dense masses of cemented tubes into millimetric clasts, which were then buried and cemented by sparry siderite.

This proposed mineralization process is provisional pending further study and verification.

4.4. Biomineralization

Calcified skeletons of invertebrate groups became relatively common in the late Ediacaran and Early Cambrian (Penny et al., 2014; Wood, 2018; Murdock, 2020), and possible calcified algae have been reported from the Cryogenian (Horodyski and Mankiewicz, 1990). Earlier Neoproterozoic records of biomineralization include phosphatic and siliceous scales (Allison and Hilgert, 1986; Macdonald et al., 2010; Cohen et al., 2011, 2017; Morais et al., 2017; Riedman et al., 2021) and vase-shaped tests (Porter and Knoll, 2000; Porter et al., 2003), especially since ~800 Ma. In addition to providing support to the organisms, these adaptations could reflect defensive mechanisms (Bengtson, 1994; Porter, 2011). In contrast to these examples, *Xiamalingella* was a key development that provides evidence for earlier biomineralization, even if it reflects essentially passive interaction between the organism and ambient aquatic chemistry. Cyanobacteria produced similar calcified tubes during the Cambrian (Elicki, 1999). It is also possible to regard *Xiamalingella* siderite tubes (Figs. 4 and 5) as an example of protective preadaptation (Simpson, 1944; Gould and Vrba, 1982) against future small herbivorous metazoans (Butterfield, 1997), for which cyanobacteria may subsequently have become prey, e.g., in the Neoproterozoic.

In vivo cyanobacterial sheath calcification has been regarded as evidence of CCMs (Kah and Riding, 2007; Liu et al., 2020b). Photosynthetic processes such as CCM may be linked to relatively low levels of atmospheric CO_2, possibly less than ~12 × preindustrial atmospheric level (PIAL, 280 ppmv; Riding, 2006), consistent with the empirical estimates of coeval CO_2 levels based on paleosols (Sheldon, 2006). Primary siderite mineralization of cyanobacteria has not been described before. It offers a plausible explanation for preferential synsedimentary preservation of the relatively resilient sheath, comparable with the preservation observed in calcification.

5. Systematic paleontology

5.1. Taxonomy

Genus: *Xiamalingella* gen. nov.
Diagnosis: Tubular filaments, circular in cross-section, non-septate, sinuous; walls smooth, thin, fine-grained; juxtaposed and interlaced, with mutually parallel to transverse orientation; forming unattached bundles that appear to be fragments; preserved in siderite grainstone (Figs. 4 and 5).

Type species: *Xiamalingella sideria* sp. nov.
Holotype. Specimen number: 1911TLZ-04, repository in the National Infrastructure of Mineral, Rock and Fossil for Science and Technology, Beijing.
Paratype. Specimen number: 1911TLZ-08, repository in the National Infrastructure of Mineral, Rock and Fossil for Science and Technology, Beijing.
Name: From its location and inferred syn-depositional siderite composition.

Historically, different names have been given to filamentous cyanobacterium-like fossils based on their mineralization as well as morphology. Examples are *Siphonophycus* (typically silicified), *Obruchevella* and *Spirellus* (typically phosphatized and helically coiled) (Peel, 1988; Min et al., 2020), and *Girvanella* (defined as a calcified fossil). Thus, in these cases, mineral composition can be part of the diagnosis. This somewhat idiosyncratic approach may be justified if calcification, as in *Girvanella*, occurred during life as a result of bioinduced calcification, and preserves a specific part of the organism (in this case the sheath). This may contrast with synsedimentary/early diagenetic phosphatization and silicification. Here we name this siderite sheath-like fossil *Xiamalingella*.

Description: As for the genus. In addition to being generally sub-parallel, tubes are locally tangled and oriented transverse to one another.

Filament dimensions: External D = 11 μm—52 μm (mean 27 μm, n = 60). Internal diameter 3 μm—36 μm (mean 16 μm); wall thickness 3 μm—10 μm (mean 6 μm) (Figs. 4, 5 and 7; Supplementary Table S1). [Type *Girvanella* External D = 35 μm—42 μm (Nicholson and Etheridge, 1878)].

Material: 25 specimens.

Remarks: In morphology and individual tube size, *Xiamalingella* resembles *Girvanella* (Nicholson and Etheridge, 1878), but is distinct in its bundled
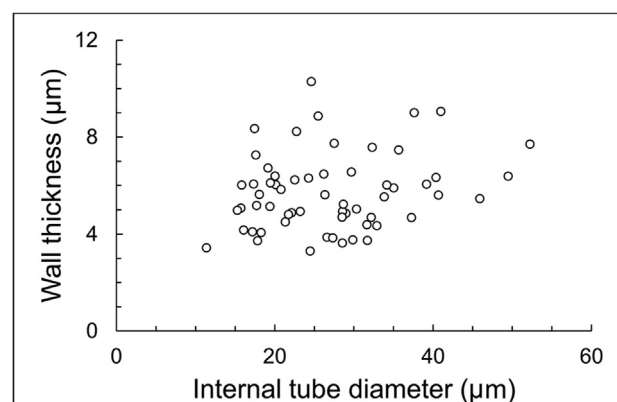

Fig. 7 *Xiamalingella sideria* dimensions from the Jixian section, based on 60 individual tubes in 5 well preserved samples.

arrangement. In this respect it resembles the cable-like arrangement of *Subtifloria* (Maslov, 1956), which is common in the Lower Cambrian (Elicki, 1999), and its junior synonym *Botominella Reitlinger* (Riding and Voronova, 1984), but it may also differ in locally having tubes oriented transverse to one another (Figs. 4 and 5).

Occurrence: Present in 25 thin sections of a total of 25 samples from one locality.

Type-locality: Tielingzi village, Jixian, Tianjin, northern China.

Geological horizon: Lower part of Member I of the Xiamaling Formation.

Age: ~1.42—1.33 Ga (see **2 Geological setting**).

Lithology and depositional environment: Grainstone composed of bioclastic siderite, deposited in offshore transitional zone below fair-weather wave base.

5.2. Comparisons

In overall size and shape, *Xiamalingella* (Figs. 4, 5 and 7; Supplementary Table S1) not only broadly resembles relatively large cyanobacteria but also small green algae, such as *Cladophora* whose fossil record can be traced back to at least to ~1 Ga (Tang *et al.*, 2020b). However, in addition to more complicated morphologic features, *Cladophora*-like algae usually also show well-defined branching, and can be up to 100 microns or more in diameter (Boedeker *et al.*, 2018). Furthermore, although *Cladophora* can be preserved by being encrusted by $CaCO_3$ during life, e.g., in non-marine tufa deposits (Riding, 1979; Bosence and Gallois, 2021), this calcification is external to the organic material and irregular, and does not usually present the appearance of being a distinct calcified 'wall' of even thickness.

The general size, circular cross-section, well-defined wall, non-septate character, and lack of branching in *Xiamalingella* (Figs. 4, 5 and 7) all broadly resemble similar features in calcified fossils interpreted as cyanobacterial sheaths that belong to the *Girvanella* Group (Riding, 1991, p. 66). In particular, *Xiamalingella* is similar to apparently unbranched forms with filaments arranged in closely juxtaposed aligned cable-like 'bundles', such as *Subtifloria*, best known from the Cambrian—Ordovician (cf. Riding and Fan, 2001, Figure 3d). Paleozoic *Subtifloria* filaments range in internal diameter up to ~20 μm (Riding and Fan, 2001, Figure 5) and ~39 μm (Feng *et al.*, 2010) in external diameter.

In the same region of northern China, cyanobacterial fossils in the ~1.58 Ga (Tian *et al.*, 2015) Gaoyuzhuang Formation include sheath-like *Siphonophycus*, *Palaeolyngbya* and *Obruchevella* (Zhang and Li, 1985; Shi *et al.*, 2017; Zhao *et al.*, 2020). Silicified multi-trichomous cyanobacteria resembling *Schizothrix* and *Microcoleus* have been reported from the lower part of the Gaoyuzhuang Formation (Seong-Joo and Golubic, 1998). In shape and arrangement, the genus *Xiamalingella* (Figs. 4 and 5) resembles some silicified fossils referred to *Siphonophycus*, such as those described by Zhao *et al.* (2020, figures 4b and 6f), from Member I of the Gaoyuzhuang Formation and Member III of the Wumishan Formation. *Siphonophycus*, widely reported from the Precambrian, is generally identified as cyanobacterial sheaths (Bartley, 1996; Schopf, 2006; Sergeev *et al.*, 2012), although these fossils might have been produced by other similarly shaped-microbes. Our *Xiamalingella* specimens range 5 μm—37 μm (mean 16 μm) in internal diameter. In this respect, they are somewhat larger than *Siphonophycus*, including examples described from the Jixian Group, and similar in size to relatively large examples of *Girvanella* (Fournie, 1967, table II), which is common in the Paleozoic.

Filamentous cyanobacteria have a protective tubular sheath that encloses strands of cells (trichomes). Some filamentous cyanobacteria have one trichome within the sheath whereas multi-trichomous filaments have several, sometimes many, trichomes within a single sheath. Seong-Joo and Golubic (1998) suggested that the appearance of multi-trichomous organization ~1.58 Ga could represent a significant step in cyanobacterial evolution (see Tosti and Riding, 2017, figure 20). However, even the widest multi-trichomous sheaths of *Eoschizothrix* described by Seong-Joo and Golubic (1998, p. 181) do not exceed ~11 μm in diameter. Nonetheless, ~1.2 Ga Dismal Lakes Formation sheaths regarded as multi-trichomous are 18 μm—36 μm in diameter (Horodyski and Donaldson, 1980, p. 136 and p. 154). We cannot tell whether *Xiamalingella* was multi-trichomous, since only the sheath appears to be preserved, but this possibility could help to account for its relatively large diameter, and would be consistent with its age.

There is a long and diverse record of Archean and Proterozoic cyanobacterium-like fossils (e.g., Horodyski and Donaldson, 1980, 1983; Yun, 1981; Knoll *et al.*, 1988, 1989; Schopf, 1992, 2006; Sergeev et al., 1995, 2002; Bartley, 1996; Demoulin *et al.*, 2019), mainly preserved in chert, and some in phosphate. Silicified sheath-like Proterozoic fossils referred to cyanobacteria can be common, for example *Anhuithrix*, *Obruchevella*, *Palaeolyngbya*, *Siphonophycus* (Schopf, 1968; Sergeev *et al.*, 1994; Sergeev and Schopf, 2010; Demoulin *et al.*, 2019, table I). In contrast, only a few occurrences of calcified

cyanobacterial sheaths are known from the Precambrian (summary in Riding, 2012). The oldest reported well-preserved examples that appear to have been originally calcified are from the latest Archean (2.52 Ga) Gamohaan Formation, South Africa (Klein *et al.*, 1987). These 15—25-μm-diameter filaments are mainly silicified, but retain a few percent ferroan dolomite that preserves the outlines of aragonite-like crystals, suggesting that they could originally have been carbonate-encrusted cyanobacterial sheaths (Klein *et al.*, 1987). Although numerous cyanobacterium-like Archean fossils ranging in age from ~3.5—2.5 Ga have been described (Schopf, 2006, table 2), recent assessment recognizes the oldest confirmed cyanobacterial fossils as mid-Paleoproterozoic (Demoulin *et al.*, 2019); these are silicified *Eoentophysalis belcherensis* (Hofmann, 1976) in ~2 Ga (age from Hodgskiss *et al.*, 2019) stromatolites of the Kasegalik Formation (Belcher Supergroup), Canada.

Morphology and *in vivo* mineralization of the sheath are key features that can assist the identification of fossil cyanobacteria (cf. Riding, 2006; Kah and Riding, 2007). Overall, *Xiamalingella* described here from siderite sediments in the basal Xiamaling Formation resembles the external protective sheaths of filamentous cyanobacteria, and is sufficiently large to permit the possibility that it was multi-trichomous. To our knowledge, *Xiamalingella* is the first record of a cyanobacterium-like siderite fossil.

6.   Conclusions

In size and shape, ~1.4 Ga *Xiamalingella* tubes closely resemble cyanobacterial sheaths that formed aligned mat-like aggregates. Good preservation in marine siderite ($FeCO_3$), with no sign of tube degradation, suggests early mineralization. Fe-oxyhydroxide could be expected to have precipitated in the presence of oxygen, but is not observed, and may have been entirely removed by DIR to Fe(II). A $CaCO_3$ precursor seems unlikely since little Ca^{2+} is preserved in the tube walls. Photosynthesis that involved CCM may have promoted siderite precipitation, preferentially preserving the sheath under relatively low levels of atmospheric CO_2 (<~12 × PIAL). To account for these observation-based data we propose the following sequence of events: (i) Sheaths were impregnated during life by Fe(III)-oxyhydroxide rather than by Ca-carbonate; (ii) Conversion of Fe(III) to siderite was carried out by DIR; (iii) Subsequent syn-sedimentary siderite cementation occurred under anoxic conditions in the presence of abundant

dissolved Fe(II). These ~1.42—1.33 Ga fossils could be the first cyanobacterium-like filaments preserved in siderite to be described, and provide an early example of biomineralization.

Availability of data and materials

The data that support the findings of this study are available on request from the corresponding author.

Authors' contributions

All the authors have actively participated in the preparation of the manuscript. Dong-Jie Tang: Conceptualization, Investigation, Writing, Review and Editing; Xiao-Ying Shi: Review and Editing; Xi-Qiang Zhou: Review and Editing; Robert Riding: Conceptualization, Writing, Review and Editing. All authors have read and agreed to the published version of the manuscript.

Conflicts of interest

The authors declare that they have no known competing financial interests or personal relationships that could have appeared to influence the study reported in this paper.

References

Allison, C.W., Hilgert, J.W., 1986. Scale microfossils from the Early Cambrian of northwest Canada. *Journal of Paleontology*, 60(5), 973—1015. https://doi.org/10.1017/S0022336000022538.

Arp, G., Reimer, A., Reitner, J., 2001. Photosynthesis-induced biofilm calcification and calcium concentrations in Phanerozoic oceans. *Science*, 292(5522), 1701−1704. https://doi.org/10.1126/science.1057204.

Bartley, J.K., 1996. Actualistic taphonomy of cyanobacteria: Implications for the Precambrian fossil record. *Palaios* 571−586. https://doi.org/10.2307/3515192.

Bengtson, S., 1994. The advent of animal skeletons. In: Bengtson, S. (Ed.), *Early Life on Earth*. Columbia University Press, New York, pp. 412−425.

Boedeker, C., Leliaert, F., Timoshkin, O.A., Vishnyakov, V.S., Díaz-Martínez, S., Zuccarello, G.C., 2018. The endemic Cladophorales (Ulvophyceae) of ancient Lake Baikal represent a monophyletic group of very closely related but morphologically diverse species. *Journal of Phycology*, 54(5), 616−629. https://doi.org/10.1111/jpy.12773.

Bosence, D., Gallois, A., 2021. How do thrombolites form? Multiphase construction of lacustrine microbialites, Purbeck Limestone Group, (Jurassic), Dorset, UK. *Sedimentology*, 69(2), 914−953. https://doi.org/10.1111/sed.12933.

Buick, R., Knoll, A.H., 1999. Acritarchs and microfossils from the Mesoproterozoic Bangemall Group, northwestern Australia. *Journal of Paleontology*, 73(5), 744−764. https://doi.org/10.1017/S0022336000040634.

Butterfield, N.J., 1997. Plankton ecology and the Proterozoic−Phanerozoic transition. *Paleobiology*, 23(2), 247−262. https://doi.org/10.1017/S009483730001681X.

Cohen, A.L., McConnaughey, T.A., 2003. Geochemical perspectives on coral mineralization. *Reviews in Mineralogy and Geochemistry*, 54(1), 151−187. https://doi.org/10.2113/0540151.

Cohen, P.A., Schopf, J.W., Butterfield, N.J., Kudryavtsev, A.B., Macdonald, F.A., 2011. Phosphate biomineralization in mid-Neoproterozoic protists. *Geology*, 39(6), 539−542. https://doi.org/10.1130/G31833.1.

Cohen, P.A., Strauss, J.V., Rooney, A.D., Sharma, M., Tosca, N., 2017. Controlled hydroxyapatite biomineralization in an ~810 million-year-old unicellular eukaryote. *Science Advances*, 3(6), e1700095. https://doi.org/10.1126/sciadv.1700095.

Cuif, J.P., Dauphin, Y., Sorauf, J.E., 2010. *Biominerals and fossils through time*. Cambridge University Press, UK, Cambridge, p. 490.

Demoulin, C.F., Lara, Y.J., Cornet, L., François, C., Baurain, D., Wilmotte, A., Javaux, E.J., 2019. Cyanobacteria evolution: Insight from the fossil record. *Free Radical Biology and Medicine*, 140, 206−223. https://doi.org/10.1016/j.freeradbiomed.2019.05.007.

Dodd, M.S., Papineau, D., She, Z., Fogel, M.L., Nederbragt, S., Pirajno, F., 2018. Organic remains in late Palaeoproterozoic granular iron formations and implications for the origin of granules. *Precambrian Research*, 310, 133−152. https://doi.org/10.1016/j.precamres.2018.02.016.

Drake, J.L., Mass, T., Stolarski, J., Von Euw, S., van de Schootbrugge, B., Falkowski, P.G., 2020. How corals made rocks through the ages. *Global Change Biology*, 26(1), 31−53. https://doi.org/10.1111/gcb.14912.

Elicki, O., 1999. Palaeoecological significance of calcimicrobial communities during ramp evolution: An example from the Lower Cambrian of Germany. *Facies*, 41(1), 27−39. https://doi.org/10.1007/BF02537458.

Fairchild, I.J., Knoll, A.H., Swett, K., 1991. Coastal lithofacies and biofacies associated with syndepositional dolomitization and silicification (Draken Formation, Upper Riphean, Svalbard). *Precambrian Research*, 53(3−4), 165−197. https://doi.org/10.1016/0301-9268(91)90071-H.

Feng, Q., Gong, Y.M., Riding, R., 2010. Mid-Late Devonian calcified marine algae and cyanobacteria, South China. *Journal of Paleontology*, 84(4), 569−587. https://doi.org/10.1666/09-108.1.

Fournie, D., 1967. Les Porostromata du Paleozoïque. Etude bibliographique. *Bulletin Du Centre de Recherches, Pau-SNPA*, 1(1), 21−41.

Gal, A., Weiner, S., Addadi, L., 2015. A perspective on underlying crystal growth mechanisms in biomineralization: solution mediated growth versus nanosphere particle accretion. *CrystEngComm*, 17(13), 2606−2615. https://doi.org/10.1039/C4CE01474J.

Golubic, S., Seong-Joo, L., 1999. Early cyanobacterial fossil record: Preservation, palaeoenvironments and identification. *European Journal of Phycology*, 34(4), 339−348. https://doi.org/10.1080/09670269910001736402.

Gould, S.J., Vrba, E.S., 1982. Exaptation — A missing term in the science of form. *Paleobiology*, 8, 4−15. https://doi.org/10.1017/S0094837300004310.

HBGMR (Hebei Bureau of Geology and Mineral Resources), 1965. *Geological Map of Xinglong: K-50-XXXIV, scale 1:200,000, geological map, 1 sheet* (in Chinese).

HBGMR (Hebei Bureau of Geology and Mineral Resources), 1967. *Geological Map of Xuanhua: K-50-XXXII, scale 1:200,000, geological map, 1 sheet* (in Chinese).

Heimann, A., Johnson, C.M., Beard, B.L., Valley, J.W., Roden, E.E., Spicuzza, M.J., Beukes, N.J., 2010. Fe, C, and O isotope compositions of banded iron formation carbonates demonstrate a major role for dissimilatory iron reduction in ~2.5 Ga marine environments. *Earth and Planetary Science Letters*, 294(1−2), 8−18. https://doi.org/10.1016/j.epsl.2010.02.015.

Hodgskiss, M.S., Dagnaud, O.M., Frost, J.L., Halverson, G.P., Schmitz, M.D., Swanson-Hysell, N.L., Sperling, E.A., 2019. New insights on the Orosirian carbon cycle, early Cyanobacteria, and the assembly of Laurentia from the Paleoproterozoic Belcher Group. *Earth and Planetary Science Letters*, 520, 141−152. https://doi.org/10.1016/j.epsl.2019.05.023.

Hofmann, H.J., 1976. Precambrian microflora, Belcher Islands, Canada: significance and systematics. *Journal of Paleontology* 1040−1073.

Horodyski, R.J., Donaldson, J.A., 1980. Microfossils from the Middle Proterozoic Dismal Lakes groups, arctic Canada. *Precambrian Research*, 11(2), 125−159. https://doi.org/10.1016/0301-9268(80)90043-1.

Horodyski, R.J., Donaldson, J.A., 1983. Distribution and significance of microfossils in cherts of the Middle Proterozoic Dismal Lakes Group, District of Mackenzie, Northwest Territories, Canada. *Journal of Paleontology*, 57(2), 271−288. https://doi.org/10.2307/1304652.

Horodyski, R.J., Mankiewicz, C., 1990. Possible Late Proterozoic skeletal algae from the Pahrump Group, Kingston Range, southeastern California. *American Journal of Science*, 290, 149—169.

Kah, L.C., Riding, R., 2007. Mesoproterozoic carbon dioxide levels inferred from calcified cyanobacteria. *Geology*, 35(9), 799—802. https://doi.org/10.1130/G23680A.1.

Kempe, S., Kazmierczak, J., 1994. The role of alkalinity in the evolution of ocean chemistry, organization of living systems, and biocalcification processes. *Bulletin de La Institut Océanographique (Monaco)*, 13, 61—117.

Klein, C., Beukes, N.J., Schopf, J.W., 1987. Filamentous microfossils in the early Proterozoic Transvaal Supergroup: Their morphology, significance, and paleoenvironmental setting. *Precambrian Research*, 36(1), 81—94. https://doi.org/10.1016/0301-9268(87)90018-0.

Knoll, A.H., Swett, K., Mark, J., 1991. Paleobiology of a Neoproterozoic tidal flat/lagoonal complex: the Draken Conglomerate Formation, Spitsbergen. *Journal of Paleontology* 531—570. https://doi.org/10.1017/S0022336000030663.

Knoll, A.H., 2003. Biomineralization and evolutionary history. *Reviews in Mineralogy and Geochemistry*, 54(1), 329—356. https://doi.org/10.2113/0540329.

Knoll, A.H., Ohta, Y., 1988. Microfossils in metasediments from Prins Karls Forland, western Svalbard. *Polar Research*, 6(1), 59—67.

Knoll, A.H., Strother, P.K., Rossi, S., 1988. Distribution and diagenesis of microfossils from the Lower Proterozoic Duck Creek Dolomite, Western Australia. *Precambrian Research*, 38(3), 257—279. https://doi.org/10.1016/0301-9268(88)90005-8.

Knoll, A.H., Swett, K., Burkhardt, E., 1989. Paleoenvironmental distribution of microfossils and stromatolites in the Upper Proterozoic Backlundtoppen Formation, Spitsbergen. *Journal of Paleontology*, 63(2), 129—145. https://doi.org/10.1017/S002233600001917X.

Knoll, A.H., Fairchild, I.J., Swett, K., 1993. Calcified microbes in Neoproterozoic carbonates: implications for our understanding of the Proterozoic/Cambrian transition. *Palaios* 512—525. https://doi.org/10.2307/3515029.

Krajina, B.A., Proctor, A.C., Schoen, A.P., Spakowitz, A.J., Heilshorn, S.C., 2018. Biotemplated synthesis of inorganic materials: An emerging paradigm for nanomaterial synthesis inspired by nature. *Progress in Materials Science*, 91, 1—23. https://doi.org/10.1016/j.pmatsci.2017.08.001.

Leadbeater, B.S., Riding, R., 1986. *Biomineralization in lower plants and animals. The Systematics Association*, 30. Clarendon Press, Oxford.

Lis, H., Shaked, Y., 2009. Probing the bioavailability of organically bound iron: A case study in the Synechococcus-rich waters of the Gulf of Aqaba. *Aquatic Microbial Ecology*, 56(2—3), 241—253. https://doi.org/10.3354/ame01347.

Liu, A., Tang, D., Shi, X., Zhou, X., Zhou, L., Shang, M., Li, Y., Fang, H., 2020a. Mesoproterozoic oxygenated deep seawater recorded by early diagenetic carbonate concretions from the Member IV of the Xiamaling Formation, North China. *Precambrian Research*, 341, 105667. https://doi.org/10.1016/j.precamres.2020.105667.

Liu, A.Q., Tang, D.J., Shi, X.Y., Zhou, L.M., Zhou, X.Q., Shang, M.H., Li, Y., Song, H.Y., 2019. Growth mechanisms and environmental implications of carbonate concretions from the ~1.4 Ga Xiamaling Formation, North China. *Journal of Palaeogeography*, 8(1), 1—16. https://doi.org/10.1186/s42501-019-0036-4.

Liu, L., Liang, L., Wu, Y., Zhou, X., Jia, L., Riding, R., 2020b. Ordovician cyanobacterial calcification: A marine fossil proxy for atmospheric CO_2. *Earth and Planetary Science Letters*, 530, 115950. https://doi.org/10.1016/j.epsl.2019.115950.

Livingston, B.T., Killian, C.E., Wilt, F., Cameron, A., Landrum, M.J., Ermolaeva, O., Sapojnikov, V., Maglott, D.R., Buchanane, A.M., Ettensohn, C.A., 2006. A genome-wide analysis of biomineralization-related proteins in the sea urchin *Strongylocentrotus purpuratus*. *Developmental Biology*, 300(1), 335—348. https://doi.org/10.1016/j.ydbio.2006.07.047.

Lowenstam, H.A., Weiner, S., 1989. Biomineralization processes. In: *On biomineralization*. Oxford University Press.

Luo, G., Hallmann, C., Xie, S., Ruan, X., Summons, R.E., 2015. Comparative microbial diversity and redox environments of black shale and stromatolite facies in the Mesoproterozoic Xiamaling Formation. *Geochimica et Cosmochimica Acta*, 151, 150—167.

Lyu, D., Deng, Y., Wang, H., Zhang, F., Ren, R., Gao, Z., Zhou, C., Luo, Z., Wang, X., Bi, L., Zhang, S., Canfield, D.E., 2021. Using cyclostratigraphic evidence to define the unconformity caused by the Mesoproterozoic Qinyu Uplift in the North China Craton. *Journal of Asian Earth Sciences*, 206, 104608. https://doi.org/10.1016/j.jseaes.2020.104608.

Ma, J., Shi, X., Lechte, M., Zhou, X., Wang, Z., Huang, K., Rudmin, M., Tang, D., 2022. Mesoproterozoic seafloor authigenic glauconite-berthierine: Indicator of enhanced reverse weathering on early Earth. *American Mineralogist*, 107(1), 116—130. https://doi.org/10.2138/am-2021-7904.

Macdonald, F.A., Cohen, P.A., Dudás, F.Ő., Schrag, D.P., 2010. Early Neoproterozoic scale microfossils in the lower Tindir Group of Alaska and the Yukon Territory. *Geology*, 38(2), 143—146. https://doi.org/10.1130/G25637.1.

Mankiewicz, C., 1992. Obruchevella and other microfossils in the Burgess Shale: preservation and affinity. *Journal of Paleontology*, 66(5), 717—729. https://doi.org/10.1017/S0022336000020758.

Mann, S., 1988. Molecular recognition in biomineralization. *Nature*, 332(6160), 119—124. https://doi.org/10.1038/332119a0.

Mann, S., 2001. *Biomineralization: Principles and concepts in bioinorganic materials chemistry*. Oxford University Press, pp. 1—198.

Maslov, V.P., 1956. The fossil calcareous algae of the USSR: Transactions of the USSR Academy of Sciences. *Geological Science Sections*, 160, 1—301 (in Russian).

Meldrum, F.C., 2003. Calcium carbonate in biomineralisation and biomimetic chemistry. *International Materials*

Reviews, 48(3), 187–224. https://doi.org/10.1179/095066003225005836.

Meng, Q.R., Wei, H.H., Qu, Y.Q., Ma, S.X., 2011. Stratigraphic and sedimentary records of the rift to drift evolution of the northern North China craton at the Paleo- to Mesoproterozoic transition. *Gondwana Research*, 20(1), 205–218. https://doi.org/10.1016/j.gr.2010.12.010.

Merz, M.U., 1992. The biology of carbonate precipitation by cyanobacteria. *Facies*, 26(1), 81–101. https://doi.org/10.1007/BF02539795.

Merz-Preiß, M., Riding, R., 1999. Cyanobacterial tufa calcification in two freshwater streams: Ambient environment, chemical thresholds and biological processes. *Sedimentary Geology*, 126(1–4), 103–124. https://doi.org/10.1016/S0037-0738(99)00035-4.

Min, X., Hua, H., Liu, L., Sun, B., Cui, Z., Dai, Q., 2020. A diverse calcified cyanobacteria assemblage in the latest Ediacaran. *Precambrian Research*, 342, 105669. https://doi.org/10.1016/j.precamres.2020.105669.

Moore, K.R., Bosak, T., Macdonald, F., Du, K., Newman, S.A., Lahr, D.J., Pruss, S.B., 2017. Pyritized Cryogenian cyanobacterial fossils from arctic Alaska. *Palaios*, 32(12), 769–778. https://doi.org/10.2110/palo.2017.063.

Morais, L., Fairchild, T.R., Lahr, D.J., Rudnitzki, I.D., Schopf, J.W., Garcia, A.K., Kudryavtsev, A.B., Romero, G.R., 2017. Carbonaceous and siliceous Neoproterozoic vase-shaped microfossils (Urucum Formation, Brazil) and the question of early protistan biomineralization. *Journal of Paleontology*, 91(3), 393–406. https://doi.org/10.1017/jpa.2017.16.

Murdock, D.J., 2020. The 'biomineralization toolkit' and the origin of animal skeletons. *Biological Reviews*, 95(5), 1372–1392. https://doi.org/10.1111/brv.12614.

Nicholson, H.A., Etheridge, R., 1878. *A Monograph of the Silurian Fossils of the Girvan District in Ayrshire with Special Reference to Those Contained in the "Grey Collection*, 1. W. Blackwood and Sons, Edinburgh.

Peel, J.S., 1988. Spirellus and related helically coiled microfossils (cyanobacteria) from the Lower Cambrian of North Greenland. *Rapport Grønlands Geologiske Undersøgelse*, 137, 5–32. https://doi.org/10.34194/rapggu.v137.8009.

Penny, A.M., Wood, R., Curtis, A., Bowyer, F., Tostevin, R., Hoffman, K.H., 2014. Ediacaran metazoan reefs from the Nama Group, Namibia. *Science*, 344(6191), 1504–1506. https://doi.org/10.1126/science.1253393.

Pentecost, A., 2005. *Travertine*. Springer, Berlin.

Planavsky, N., Reid, R.P., Lyons, T.W., Myshrall, K.L., Visscher, P.T., 2009. Formation and diagenesis of modern marine calcified cyanobacteria. *Geobiology*, 7(5), 566–576. https://doi.org/10.1111/j.1472-4669.2009.00216.x.

Porter, S., 2011. The rise of predators. *Geology*, 39(6), 607–608. https://doi.org/10.1130/focus062011.1.

Porter, S.M., Knoll, A.H., 2000. Testate amoebae in the Neoproterozoic Era: evidence from vase-shaped microfossils in the Chuar Group, Grand Canyon. *Paleobiology*, 26(3), 360–385. https://doi.org/10.1666/0094-8373(2000)026<0360:TAITNE>2.0.CO, 2.

Porter, S.M., Meisterfeld, R., Knoll, A.H., 2003. Vase-shaped microfossils from the Neoproterozoic Chuar Group, Grand Canyon: A classification guided by modern testate amoebae. *Journal of Paleontology*, 77(3), 409–429. https://doi.org/10.1666/0022-3360(2003)077<0409:VMFTNC>2.0.CO, 2.

Riding, R., 2006. Cyanobacterial calcification, carbon dioxide concentrating mechanisms, and Proterozoic–Cambrian changes in atmospheric composition. *Geobiology*, 4(4), 299–316. https://doi.org/10.1111/j.1472-4669.2006.00087.x.

Riding, R., 1979. Origin and diagenesis of lacustrine algal bioherms at the margin of the Ries crater, Upper Miocene, southern Germany. *Sedimentology*, 26(5), 645–680. https://doi.org/10.1111/j.1365-3091.1979.tb00936.x.

Riding, R., 1991. Calcified cyanobacteria. In: *Calcareous Algae and Stromatolites*. Springer, Berlin, pp. 55–87.

Riding, R., 2012. A hard life for cyanobacteria. *Science*, 336(6080), 427–428. https://doi.org/10.1126/science.1221055.

Riding, R., Fan, J., 2001. Ordovician calcified algae and cyanobacteria, northern Tarim Basin subsurface, China. *Palaeontology*, 44(4), 783–810. https://doi.org/10.1111/1475-4983.00201.

Riding, R., Voronova, L., 1984. Assemblages of calcareous algae near the Precambrian/Cambrian boundary in Siberia and Mongolia. *Geological Magazine*, 121(3), 205–210. https://doi.org/10.1017/S0016756800028260.

Riedman, L.A., Porter, S.M., Czaja, A.D., 2021. Phosphatic scales in vase-shaped microfossil assemblages from Death Valley, Grand Canyon, Tasmania, and Svalbard. *Geobiology*, 19(4), 364–375. https://doi.org/10.1111/gbi.12439.

Rose, A.L., Waite, T.D., 2005. Reduction of organically complexed ferric iron by superoxide in a simulated natural water. *Environmental Science and Technology*, 39(8), 2645–2650. https://doi.org/10.1021/es048765k.

Rudolf, M., Kranzler, C., Lis, H., Margulis, K., Stevanovic, M., Keren, N., Schleiff, E., 2015. Multiple modes of iron uptake by the filamentous, siderophore-producing cyanobacterium, *Anabaena* sp. PCC 7120. *Molecular Microbiology*, 97(3), 577–588. https://doi.org/10.1111/mmi.13049.

Schopf, J.W., 1968. Microflora of the Bitter Springs Formation, late Precambrian, central Australia. *Journal of Paleontology*, 42(3), 651–688.

Schopf, J.W., 1992. Proterozoic prokaryotes: Affinities, geologic distribution, and evolutionary trends. In: Schopf, J.W., Klein, C. (Eds.), *The Proterozoic Biosphere: A Multidisciplinary Study*. Cambridge University Press, UK, Cambridge, pp. 195–218.

Schopf, J., 2006. Fossil evidence of Archaean life. *Philosophical Transactions of the Royal Society B: Biological Sciences*, 361(1470), 869–885. https://doi.org/10.1098/rstb.2006.1834.

Seong-Joo, L., Golubic, S., 1998. Multi-trichomous cyanobacterial microfossils from the Mesoproterozoic Gaoyuzhuang Formation, China: Paleoecological and taxonomic implications. *Lethaia*, 31(3), 169–184. https://doi.org/10.1111/j.1502-3931.1998.tb00505.x.

Sergeev, V.N., Knoll, A.H., Grotzinger, J.P., 1995. Paleobiology of the Mesoproterozoic Billyakh Group, Anabar uplift, northern Siberia. *Journal of Paleontology,* 69(S39), 1—37. https://doi.org/10.1017/S0022336000062375.

Sergeev, V.N., Knoll, A.H., Kolosova, S.P., Kolosov, P.N., 1994. Microfossils in cherts from the Mesoproterozoic (Middle Riphean) Debengda Formation, the Olenek Uplift, northeastern Siberia. *Stratigraphy and Geological Correlation,* 2(1), 19—33.

Sergeev, V.N., Gerasimenko, L.M., Zavarzin, G.A., 2002. The Proterozoic history and present state of cyanobacteria. *Microbiology,* 71(6), 623—637. https://doi.org/10.1023/A:1021415503436.

Sergeev, V.N., Sharma, M., Shukla, Y., 2012. Proterozoic fossil cyanobacteria. *Palaeobotanist,* 61, 189—358.

Sergeev, V.N., Schopf, J.W., 2010. Taxonomy, paleoecology and biostratigraphy of the late Neoproterozoic Chichkan microbiota of South Kazakhstan: The marine biosphere on the eve of metazoan radiation. *Journal of Paleontology,* 84(3), 363—401. https://doi.org/10.1666/09-133.1.

She, Z., Strother, P., McMahon, G., Nittler, L.R., Wang, J., Zhang, J., Sang, L., Ma, C., Papineau, D., 2013. Terminal Proterozoic cyanobacterial blooms and phosphogenesis documented by the Doushantuo granular phosphorites I: *In situ* micro-analysis of textures and composition. *Precambrian Research,* 235, 20—35. https://doi.org/10.1016/j.precamres.2013.05.011.

Sheldon, N.D., 2006. Precambrian paleosols and atmospheric CO_2 levels. *Precambrian Research,* 147(1—2), 148—155. https://doi.org/10.1016/j.precamres.2006.02.004.

Shi, M., Feng, Q., Khan, M.Z., Zhu, S., 2017. An eukaryote-bearing microbiota from the early Mesoproterozoic Gaoyuzhuang Formation, Tianjin, China and its significance. *Precambrian Research,* 303, 709—726. https://doi.org/10.1016/j.precamres.2017.09.013.

Simpson, G.G., 1944. *Tempoand Mode in Evolution.* Columbia University Press, New York City, NY, USA. 217 pages, 36 figures, 19 tables.

Stefurak, E.J., Lowe, D.R., Zentner, D., Fischer, W.W., 2014. Primary silica granules — A new mode of Paleoarchean sedimentation. *Geology,* 42(4), 283—286. https://doi.org/10.1130/G35187.1.

Swanner, E.D., Bayer, T., Wu, W., Hao, L., Obst, M., Sundman, A., Byrne, J.M., Michel, F.M., Kleinhanns, I.C., Kappler, A., Schoenberg, R., 2017. Iron isotope fractionation during Fe (II) oxidation mediated by the oxygen-producing marine cyanobacterium *Synechococcus* PCC 7002. *Environmental Science and Technology,* 51(9), 4897—4906. https://doi.org/10.1021/acs.est.6b05833.

Swett, K., Knoll, A.H., 1985. Stromatolitic bioherms and microphytolites from the late Proterozoic Draken Conglomerate Formation, Spitsbergen. *Precambrian Research,* 28(3—4), 327—347. https://doi.org/10.1016/0301-9268(85)90037-3.

Tang, D., Shi, X., Jiang, G., Zhou, X., Shi, Q., 2017. Ferruginous seawater facilitates the transformation of glauconite to chamosite: An example from the Mesoproterozoic Xiamaling Formation of North China.

American Mineralogist, 102(11), 2317—2332. https://doi.org/10.2138/am-2017-6136.

Tang, D., Shi, X., Jiang, G., Wu, T., Ma, J., Zhou, X., 2018. Stratiform siderites from the Mesoproterozoic Xiamaling Formation in North China: Genesis and environmental implications. *Gondwana Research,* 58, 1—15. https://doi.org/10.1016/j.gr.2018.01.013.

Tang, D., Ma, J., Shi, X., Lechte, M., Zhou, X., 2020a. The formation of marine red beds and iron cycling on the Mesoproterozoic North China Platform. *American Mineralogist,* 105(9), 1412—1423. https://doi.org/10.2138/am-2020-7406.

Tang, Q., Pang, K., Yuan, X., Xiao, S., 2020b. A one-billion-year-old multicellular chlorophyte. *Nature Ecology & Evolution,* 4(4), 543—549. https://doi.org/10.1038/s41559-020-1122-9.

Thompson, J.B., Ferris, F.G., 1990. Cyanobacterial precipitation of gypsum, calcite, and magnesite from natural alkaline lake water. *Geology,* 18(10), 995—998. https://doi.org/10.1130/0091-7613(1990)018<0995:CPOGCA>2.3.CO, 2.

Thorne, R.J., Schneider, K., Hu, H., Cameron, P.J., 2015. Iron reduction by the cyanobacterium *Synechocystis* sp. PCC 6803. *Bioelectrochemistry,* 105, 103—109. https://doi.org/10.1016/j.bioelechem.2015.05.015.

Tian, H., Zhang, J., Li, H., Su, W., Zhou, H., Yang, L., Xiang, Z., Geng, J., Liu, H., Zhu, S., Xu, Z., 2015. Zircon LA—MC—ICPMS U—Pb dating of tuff from Mesoproterozoic Gaoyuzhuang Formation in Jixian County of North China and its geological significance. *Acta Geoscientica Sinica,* 36(5), 647—658 (in Chinese with English Abstract).

Tosti, F., Riding, R., 2017. Fine-grained agglutinated elongate columnar stromatolites: Tieling Formation, ca 1420 Ma, North China. *Sedimentology,* 64(4), 871—902. https://doi.org/10.1111/sed.12336.

Turner, E.C., 2009. Mesoproterozoic carbonate systems in the Borden Basin, Nunavut. *Canadian Journal of Earth Sciences,* 46(12), 915—938. https://doi.org/10.1139/E09-062.

Turner, E.C., 2021. Possible poriferan body fossils in Early Neoproterozoic microbial reefs. *Nature,* 596(7870), 87—91. https://doi.org/10.1038/s41586-021-03773-z.

Turner, E.C., Narbonne, G.M., James, N.P., 1993. Neoproterozoic reef microstructures from the Little Dal Group, northwestern Canada. *Geology,* 21(3), 259—262. https://doi.org/10.1130/0091-7613(1993)021<0259:NRMFTL>2.3.CO, 2.

Viney, C., 2004. Self-assembly as a route to fibrous materials: Concepts, opportunities and challenges. *Current Opinion in Solid State & Materials Science,* 8(2), 95—101. https://doi.org/10.1016/j.cossms.2004.04.001.

Weiner, S., Dove, P.M., 2003. An overview of biomineralization processes and the problem of the vital effect. *Reviews in Mineralogy and Geochemistry,* 54(1), 1—29. https://doi.org/10.2113/0540001.

Westbroek, P., De Jong, E.W., 1983. *Biomineralization and Biological Metal Accumulation. Biological and Geological Perspectives* (Papers presented at the Fourth International Symposium on Biomineralization, Renesse, The

Netherlands, June 2-5, 1982). D. Reidel Publishing Company, Dordrecht-Boston-London, pp. 1–533.

Wood, R., 2018. Exploring the drivers of early biomineralization. *Emerging Topics in Life Sciences*, 2(2), 201–212. https://doi.org/10.1042/ETLS20170164.

Wu, M.T., Fang, H., Sun, L.F., Shi, X.Y., Tang, D.J., 2021. Variations in precipitation pathways of Mesoproterozoic shallow seawater carbonates from North China Platform: Response in seawater redox fluctuations? *Journal of Palaeogeography*, 23(4), 703–722. https://doi.org/10.7605/gdlxb.2021.04.050 (in Chinese with English Abstract).

Yun, Z., 1981. Proterozoic stromatolite microfloras of the Gaoyuzhuang Formation (Early Sinian: Riphean), Hebei, China. *Journal of Paleontology* 485–506. https://www.jstor.org/stable/1304265.

Zhang, S., Wang, X., Hammarlund, E.U., Wang, H., Costa, M.M., Bjerrum, C.J., Connelly, J.N., Zhang, B., Bian, L., Canfield, D.E., 2015. Orbital forcing of climate 1.4 billion years ago. *Proceedings of the National Academy of Sciences*, 112(12), E1406–E1413. https://doi.org/10.1073/pnas.1502239112.

Zhang, S., Wang, X., Wang, H., Bjerrum, C.J., Hammarlund, E.U., Costa, M.M., Connelly, J.N., Zhang, B., Su, J., Canfield, D.E., 2016. Sufficient oxygen for animal respiration 1,400 million years ago. *Proceedings of the National Academy of Sciences*, 113(7), 1731–1736. https://doi.org/10.1073/pnas.1523449113.

Zhang, S., Wang, X., Wang, H., Bjerrum, C.J., Hammarlund, E.U., Haxen, E.R., Wen, H., Ye, Y., Canfield, D.E., 2019. Paleoenvironmental proxies and what the Xiamaling Formation tells us about the mid-Proterozoic ocean. *Geobiology*, 17(3), 225–246. https://doi.org/10.1111/gbi.12337.

Zhang, S.H., Zhao, Y., Li, X.H., Ernst, R.E., Yang, Z.Y., 2017. The 1.33–1.30 Ga Yanliao large igneous province in the North China Craton: Implications for reconstruction of the Nuna (Columbia) supercontinent, and specifically with the North Australian Craton. *Earth and Planetary Science Letters*, 465, 112–125. https://doi.org/10.1016/j.epsl.2017.02.034.

Zhang, Z., Li, S., 1985. Microflora from the Gaoyuzhuang Formation (Changchengian System) of Western Yanshan Range, North China. *Acta Micropalaeontologica Sinica*, 2, 219–230 (in Chinese with English Abstract).

Zhao, C., Shi, M., Feng, Q., Ye, Y., Khan, M.Z., Feng, F., 2020. New study of microbial mats from the Mesoproterozoic Jixian Group, North China: Evidence for photosynthesis and oxygen release. *Precambrian Research*, 344, 105734. https://doi.org/10.1016/j.precamres.2020.105734.

Supplementary data

Supplementary data to this article can be found online at https://doi.org/10.1016/j.jop.2023.03.006.